

This is the accepted manuscript made available via CHORUS. The article has been published as:

Ultrashort Nucleic Acid Duplexes Exhibit Long Wormlike Chain Behavior with Force-Dependent Edge Effects

Kevin D. Whitley, Matthew J. Comstock, and Yann R. Chemla

Phys. Rev. Lett. **120**, 068102 — Published 9 February 2018

DOI: [10.1103/PhysRevLett.120.068102](https://doi.org/10.1103/PhysRevLett.120.068102)

Ultrashort nucleic acid duplexes exhibit long worm-like chain behavior with force-dependent edge effects

Kevin D. Whitley¹, Matthew J. Comstock^{2,3†}, Yann R. Chemla^{1,2,3*}

¹*Center for Biophysics and Quantitative Biology*, ²*Department of Physics*, ³*Center for the Physics of Living Cells*, University of Illinois, Urbana-Champaign

[†]Current address: *Department of Physics, Michigan State University, East Lansing, MI 48824*

*Correspondence: *1110 W Green St., Urbana, IL, 61801, USA*

Email: ychemla@illinois.edu

Abstract:

Despite their importance in biology and use in nanotechnology, the elastic behavior of nucleic acids on “ultrashort” (<15 nt) length scales remains poorly understood. Here, we use optical tweezers combined with fluorescence imaging to observe directly the hybridization of oligonucleotides (7-12 nt) to a complementary strand under tension and to measure the difference in end-to-end extension between the single-stranded and duplex states. Data are consistent with long-polymer models at low forces (<8 pN) but smaller than predicted at higher forces (>8 pN), the result of the sequence-dependent duplex edge effects.

The behavior of nucleic acids (NAs) under applied force is a critical determinant in numerous biological and nanotechnological systems. The mechanical and dynamic properties of NAs are critical in gene regulation [1,2] and genome compaction across multiple length scales [1-5], and NAs are subject to stretching forces by enzymes in diverse cellular processes such as replication [6], transcription [7,8], translation [9-11], and chromatin remodeling [12]. In addition, recent research has exploited the elastic behavior of NAs to engineer complex nanostructures [13], nanodevices [14-18], and force-dependent nanosensors [19,20].

Although models such as the worm-like chain (WLC) or its variants (*e.g.* extensible worm-like chain (XWLC)) describe the elastic properties of long NA duplexes well [21-24], it remains under debate which model is most appropriate—and whether a single, universal model is even sufficient—to describe short duplexes on the scale of a single persistence length and shorter ($\lesssim 150$ bp). Some experimental studies of short duplexes have described deviations from canonical WLC behavior [25-27], supporting alternative models such as the sub-elastic chain [26] and kinkable WLC [28-31], while other studies have reported no deviation from canonical, long-polymer behavior [32,33]. What model describes the elastic behavior of NA duplexes on the scale of a single helical turn (~ 10 bp), which we refer to as ‘ultrashort’ duplexes, is unclear, with only a few experimental studies reported [34,35].

Here, we used single-molecule force spectroscopy [36] to investigate the elastic behavior of ultrashort (≤ 12 nt) DNA and RNA duplexes by observing the change in end-to-end extension, $\Delta X(F)$, of a nucleic acid strand when it base-pairs with a complementary strand under force F . We tethered a DNA construct containing a single-stranded (ss)DNA segment flanked by two long (1.7-kb) double-stranded (ds)DNA ‘handles’ between two beads in optical traps (Fig. 1A). The 19-nt ssDNA segment contained two poly-dT ‘spacers’ on either side of a central binding site consisting of a random sequence to which short, complementary oligonucleotide ‘probes’ labeled with a single 3’ Cy3 fluorophore could bind (Table S1 in [37]). Using an instrument combining high-resolution optical tweezers with single-molecule confocal fluorescence microscopy [36], we detected binding (or unbinding) of the probe oligonucleotide from the stepwise increase (or decrease) in fluorescence signal detected by confocal microscopy, and we

determined the coincident extension change ΔX using the optical traps (Fig. 1B; see [37]). Fluorescence detection provided the most robust method to identify probe binding and dissociation events unambiguously even when the extension change was smaller than our optical trap noise (near 5 pN the change in extension is negligibly small, rendering it impossible to detect events with the optical traps alone). Control experiments showed that there was no systematic effect of the probe fluorophore on the measured extension change (Fig. S1 in [37]). ΔX was measured as a function of tension F on the tethered DNA strand and for different probe lengths ($\ell = 8, 9, 10, 12$ nt). The measured extension changes for binding and unbinding for all probes and forces investigated were equal in magnitude within experimental error and opposite in sign (Fig. 1C). Throughout, we considered the extension change averaged over many binding and unbinding events.

Figure 2A shows the effect of tension on the extension change for all probes, scaled by probe length, $\Delta x \equiv \Delta X/\ell$. We compared these measured values to the extension change expected for long polymers, i.e. $\Delta x_{model}(F) = x_{ds}(F) - x_{ss}(F)$, where $x_{ds}(F)$ is the extension of the double-stranded state per base-pair and $x_{ss}(F)$ is the extension of the single-stranded state per nucleotide. In Fig. 2A, the shaded band represents $\Delta x_{model}(F)$ obtained from the XWLC model for $x_{ds}(F)$ [23,55] and the recently described snake-like chain (SLC) model [56] for $x_{ss}(F)$ using the most parsimonious range of parameters from the literature and empirically determined (see Table S2 and Fig. S2 in [37]). Although the measured Δx agree very well with the long-polymer model at low force ($\lesssim 10$ pN), its magnitude $|\Delta x|$ is systematically smaller than expected (*e.g.* $p < 10^{-11}$ for the 9-nt probe; see [37] and Table S3) across all probe lengths at higher forces ($\gtrsim 10$ pN), meaning that the hybridized, duplex state is closer in extension to ssDNA than predicted by the long-polymer model. We observed a similar deficit in measurements at higher ionic strengths (2 and 20 mM $[\text{Mg}^{2+}]$; Fig S3 in [37]), and an even larger deficit when replacing the DNA oligonucleotide probe with RNA (Fig. S4 in [37]).

A commonality in the measurements above was the absence of neighboring base-pairs at the edges of the bound probes in our construct design (Fig. 2A, inset). We thus designed variants of the DNA substrate lacking one ($N_{sp} = 1$) or both spacers ($N_{sp} = 0$), allowing the terminal base-pair of one or both handles to

be adjacent to those on the bound oligonucleotide probe (Fig. 2B, inset; “1Sp insert” and “0Sp insert” in Table S1 in [37]). Removal of the dT ‘spacers’ flanking the probe binding site had a significant effect on the deviation between data and model. Data from binding of a 9-nt probe on zero- and one-spacer constructs displayed significantly less of the high-force deviation observed from the construct with both spacers ($N_{sp} = 2$; Fig. 2B; “2Sp insert” in Table S1), instead showing a change in extension well in-line with that predicted by the long-polymer model. (For the zero-spacer measurement, we detected no binding of probes with 3'-attached dye, an observation we attributed to steric hindrance with the neighboring handles, and we thus used a 9-nt DNA probe that had an internally-attached dye (“9merIntCy3” in Table S1)). These results demonstrate that the deviation from the predicted elastic behavior at high force is strongly affected by the terminal base-pairs of the hybridized probe.

We also investigated whether the sequence of the terminal base-pairs affected the deviation. We measured the extension changes of two additional 10-nt probes with alternate sequences (Fig. 2C). These sequences were designed to have the same overall GC content as the original 10-nt probe, but with one (“seq2”; Fig. 2C inset) or two (“seq3”; Fig. 2C inset) GC pairs at each end of the duplex, which progressively increase the terminal base-pair stability. The measured extension changes for these two alternate-sequence probes were significantly different from those of the original ($p < 10^{-7}$; see Table S4 in [37]), deviating less from prediction at high forces (Fig. 2C). Comparing various probes, the deviation between measurement and long-polymer model integrated over force decreased with increasing terminal base-pair stability (Fig. S5 in [37]). Thus, the effect is localized to the duplex termini, and their energetics play an important role. Differences in the magnitude of the deviation under different ionic conditions (Fig. S5 in [37]) similarly reflect differing terminal base-pairing energies.

We next considered a simple and general model for our data. The fact that deviations from the long-polymer model vary based on the type of nucleic acid (e.g. DNA vs. RNA) while the tethered construct remains the same strongly suggests that the error must lie in our model of the duplex elasticity. Since edge effects from terminal base-pairs appear to contribute greatly to the deviation, we consider that each

duplex edge has a different force-extension behavior, $x_e(F)$, compared to the internal portion of the duplex, which we assume to follow the long-polymer XWLC model, $x_{ds}(F)$. We must account for such edge effects not only at each end of the hybridized probe but also at any other ds-ssDNA junction found on the tethered molecule (Fig. 3A). In the absence of a bound probe, the extension of the unbound (unhybridized) state, $X_u(F)$, is given by

$$X_u(F) = (2\ell_h - 2\ell_e)x_{ds}(F) + 2\ell_e x_e(F) + (\ell + N_{sp}\ell_{sp})x_{ss}(F), \quad (1)$$

where ℓ_h is the length of each dsDNA handle, ℓ_e is the number of base-pairs that comprise the edge regions with different elastic properties, ℓ is the length of probe binding site, ℓ_{sp} the spacer length, and $N_{sp} = 0, 1, 2$ is the number of spacers flanking the binding site. $x_{ds}(F)$, $x_e(F)$, and $x_{ss}(F)$ are the extensions of 1 base-pair of internal dsDNA, edge dsDNA, and 1 nucleotide of ssDNA, respectively. Upon probe binding, the bound (hybridized) state extension, $X_b(F)$, is given by

$$X_b(F) = (2\ell_h + \ell - 2N_{sp}\ell_e)x_{ds}(F) + 2N_{sp}\ell_e x_e(F) + N_{sp}\ell_{sp}x_{ss}(F) \quad (2)$$

Thus, the measured extension change is:

$$\Delta X = X_b(F) - X_u(F) = (\ell - 2(N_{sp} - 1)\ell_e)x_{ds}(F) + 2(N_{sp} - 1)\ell_e x_e(F) - \ell x_{ss}(F) \quad (3)$$

It is instructive to plot the deviation between the measured extension change and the long-polymer model, or residual (Fig. 3B). According to Eq. (3) above, the deviation should equal the following simple expression:

$$\begin{aligned} \Delta X - \Delta X_{\text{model}} &= (X_b(F) - X_u(F)) - \ell(x_{ds}(F) - x_{ss}(F)) \\ &= 2(N_{sp} - 1)\ell_e(x_e(F) - x_{ds}(F)) \end{aligned} \quad (4)$$

Eq. (4) predicts that the $N_{sp} = 1$ -spacer construct should not deviate from the long-polymer model while the 2- and 0-spacer constructs must deviate from this model in opposite directions by the same magnitude. This agrees well with observations (Fig. 3C), corroborated by statistical analysis (see Materials and Methods, Table S3 in [37]). The reason for this behavior is simple: for $N_{sp} = 1$ the same number of edges are present before and after probe binding, whereas this number changes by $\Delta N_e = +2$ in the case of $N_{sp} =$

2 spacers, and $\Delta N_e = -2$ in the case of $N_{sp} = 0$ spacers (Fig. 3A). Eq. (4) also predicts that the deviation should be the same for all probe lengths, provided ℓ_e is independent of ℓ . As shown in Fig. 3B, the measured deviations for all ℓ overlap reasonably well (see Table S4 in [37]).

We next asked what edge effects could lead to such force-dependent behavior. One possibility is simply that the terminal base-pairs of the duplex increasingly fray under force. The observation that deviations are smaller for more stable base-pairs (Fig. S5 in [37]) is consistent with fraying. We developed a simple statistical thermodynamic model similar to that of Gross et al. [57] in which the duplex can have a number of base-pairs, ℓ_e , thermally frayed from its ends. The free energy of a duplex with ℓ_e frayed base-pairs is given by:

$$\Delta G(F) = (\ell - \ell_e)g_{ds}(F) + \ell_e g_{ss}(F) + \sum_{i=-(\ell-\ell_e)/2}^{(\ell-\ell_e)/2-1} g_{bp}^{(i)} - F\Delta X. \quad (5)$$

Here, the first term represents the elastic energy of the double-stranded (*i.e.* un-frayed) portion of the duplex $\ell - \ell_e$ in length and where $g_{ds}(F)$ is the energy of stretching a single base-pair to force F , calculated using the XWLC model, the second term represents the elastic energy of the single-stranded (*i.e.* frayed) portion ℓ_e nucleotides in length, where $g_{ss}(F)$ is the energy of stretching a single nucleotide to force F , calculated using the SLC model, and the third term sums over the $\ell - \ell_e - 1$ nearest-neighbor base-pairing energies $g_{bp}^{(i)}$, values for which are taken from the literature [58,59]. The last term is the work done stretching the molecule to force F . (The terms in this expression are described in [37]). The expected deviation from the long-polymer model is given by Eq. (4) with $x_e(F) = x_{ss}(F)$ and $\ell_e = \langle \ell_e(F) \rangle$, the thermal average number of frayed base-pairs at force F . Comparing this model to our results, this fraying model fails to capture the magnitude of the deviation observed (Fig. 3B) because the difference in elastic energies of the double- and single-stranded states is not comparable to the base-pairing energies until a force of ~ 60 pN [57], much higher than the forces assayed. Over the experimental force range ($F < 25$ pN), this model predicts that the average number of frayed base-pairs $\langle \ell_e(F) \rangle < 0.5$ bp, whereas the observed deviation would require $\langle \ell_e(F) \rangle \sim 3$ bp for the highest force and longest probes assayed.

To generate the larger deviations observed, a fraying model must include other contributions destabilizing the edge base-pairs. We considered the effect of an extra force-dependent energy, $E_{extra}(F)$, added to the terminal base-pairs in Eq. (5). Figure 3D displays what this additional energy term would need to be, on average, at each force for the fraying model to match the deviations for the probes in Fig. 3B. This term was added to the ultimate and penultimate base-pairs at both edges of the duplex to allow for a sufficient number (~ 3 bp) to be frayed. As shown in Fig. 3D, this additional energy per base-pair is negligible at forces < 8 pN for the four probes examined, as expected, but then increases approximately linearly with force to a value of ~ 2.1 $k_B T$ /bp, similar to the energy of a single base-pair on average. (Analysis on the various individual probes yields a range of terminal base-pair energies from 1.5 to 2.8 $k_B T$ /bp.)

We speculate on the source of this extra energy. In our experimental configuration, tension on the tethered strand not only stretches each strand of the duplex but also generates shear, which may further destabilize the terminal base-pairs of the duplex. This effect was first considered, albeit in a different geometry, by de Gennes [60]. By describing a double-stranded DNA molecule as a network of harmonic springs, de Gennes showed that a shearing force can distort the ends of the duplex, facilitating fraying. Base-fraying is modeled by treating the interstrand springs as brittle bonds, breaking above a stretching threshold.

This model predicts the same qualitative behavior as Fig. 3D, with a force of ~ 8 pN sufficiently distorting some edge base-pairs that they fray. This value is consistent with measurements of shear-induced rupture of short duplexes [35]. Due to inherent limitations in the simple de Gennes ladder model, we cannot make a quantitative comparison between the shear-induced base-breaking it predicts and our data (see [37]). Nevertheless, we can describe the data generically using a phenomenological model for the additional energy contribution. A fit of the additional energy to a temperature-smoothed step function, $E_{extra}(F) = E_{extra}^0 / (1 + e^{-\alpha(F-F_0)/k_B T})$, recapitulates the data in Fig. 3D well, with fitted parameters $E_{extra}^0 = 2.1 \pm 0.1$ $k_B T$ /bp, $\alpha = 2.7 \pm 0.5$ nm, and $F_0 = 8.6 \pm 0.3$ pN. These values are likely to depend on

the energetics of the terminal base-pairs. For the alternate probe sequences, the data suggest that F_0 increases to $\sim 15\text{-}20$ pN for the more energetically stable terminal base-pairs (Fig. S6). These values match the reported unzipping forces for GC and AT base-pairs in nanomechanical measurements on DNA hairpins [61,62], although care should be taken comparing these values to ours, since the direction in which force was applied is different in the two measurements.

The elasticity of nucleic acids on short length scales and the range of validity of long-polymer models have been the subject of debate in recent years [25,27,29,31,32]. Our high-resolution measurements show that long-polymer models are appropriate even for nucleic acids of ultrashort lengths (<12 bp) provided forces are low (<10 pN). Above those forces, sequence-dependent edge effects, which we argue are due to distortions of the canonical base-pair structure, lead to premature fraying. We speculate that some nucleic acid-processing enzymes such as helicases may exploit this mechanism, exerting local forces to facilitate base-fraying and consequently, duplex unwinding. It may seem surprising that long-polymer models could match data over *any* range of forces at ultra-short length scales. Viewing the hybridization reaction explicitly considering the long dsDNA handles flanking the probe binding site reveals why. In the case of the 1-spacer construct, which best matches the long-polymer model at high forces, probe hybridization simply corresponds to extending a long, $\ell_h = 1.7\text{-kb}$ polymer (i.e. the right dsDNA handle) by ℓ bp. We would expect long-polymer models to match the elastic behavior of long molecules of length $\ell_h + \ell$ and ℓ_h , and thus the same for their difference. As our measurements make clear, on short length scales, edge effects—and associated sequence dependence—cannot be ignored and have a significant bearing on the elastic and force-dependent properties of nucleic acids. This may be an important consideration in the design of NA-based nanodevices and in modeling the effects of mechanical force on NAs in biological systems.

Acknowledgements

We thank members of the Chemla, Aksimentiev, and Goldenfeld laboratories for scientific discussion. Funding was provided by National Science Foundation grants MCB-0952442 (CAREER) and PHY-1430124 (Center for the Physics of Living Cells), and National Institutes of Health grant R21 RR025341.

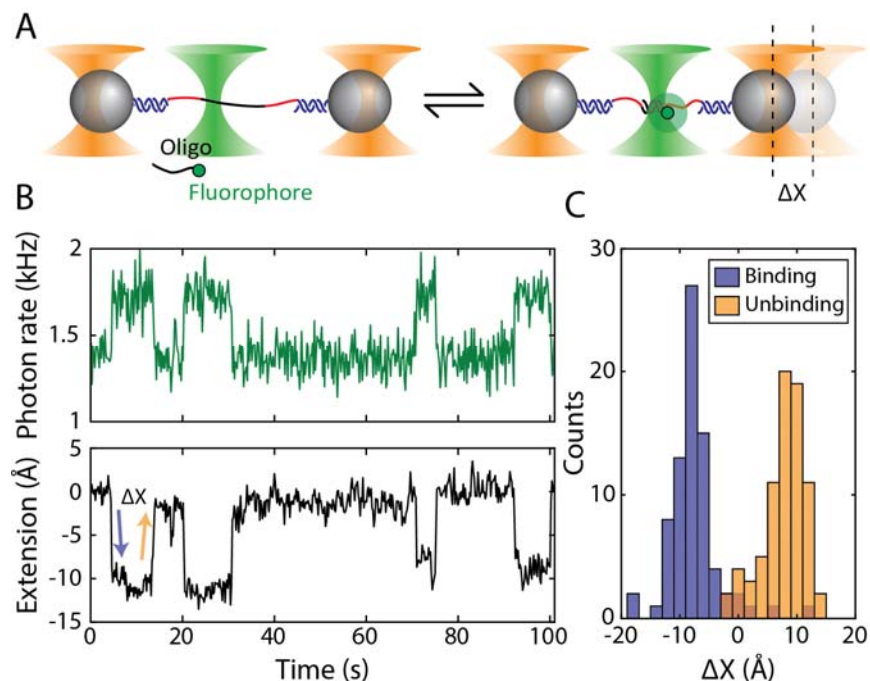


FIG. 1 (color online): Measurement of extension difference between single- and double-stranded ultrashort oligonucleotides under force. (A) Schematic of the hybridization assay (not to scale). A DNA molecule containing a short, central ssDNA region containing a binding site (*black*) flanked by poly-dT spacers (*red*) and long dsDNA handles (*blue*) is attached to polystyrene beads (*grey spheres*) in optical traps (*orange cones*) and held at a constant force. A fluorescence excitation laser (*green cone*) is focused on the central ssDNA region. Short oligonucleotides (*black*) labeled with a Cy3 fluorophore at the 3' end (*green disk*) bind and unbind to the complementary ssDNA sequence in the center of the tethered DNA. Binding and unbinding events are detected by the fluorescence emitted from the attached fluorophore and the simultaneous change in separation between the optical traps at constant force. (B) Representative time trace showing 10-nt DNA probes binding and unbinding a DNA construct held under constant force (12.4 pN). The extension difference between the single-stranded state and the double-stranded state, ΔX , is measured from the stepwise increase or decrease in the trap separation. (C) Histogram of recorded extension differences for binding and unbinding of the 10-nt probes using the hybridization assay.

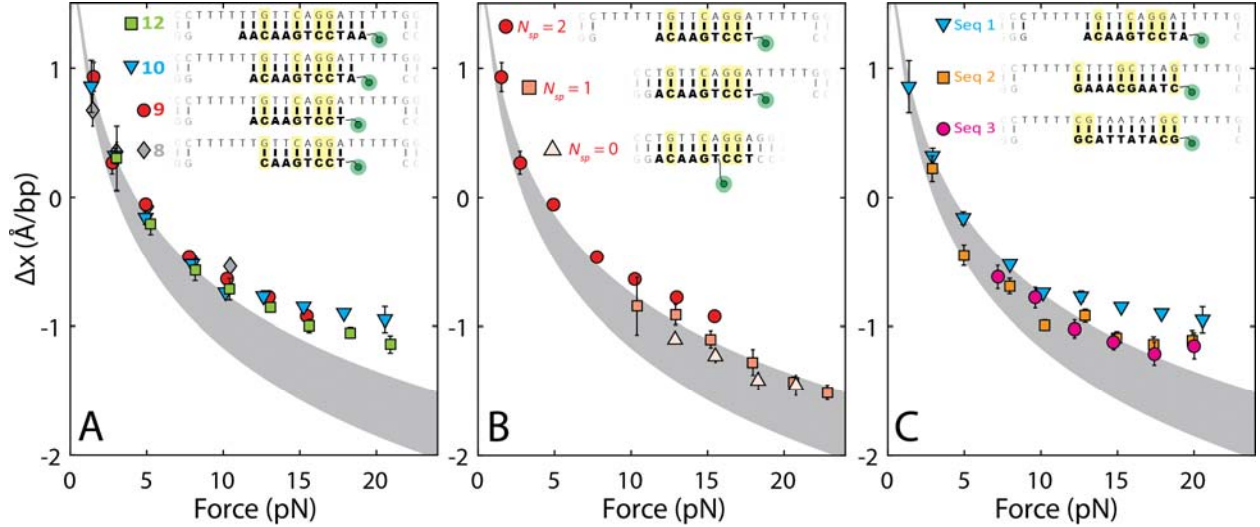


FIG. 2 (color online): Comparison of measured extension changes to long-polymer models. (A) Extension changes due to probe hybridization, scaled by probe length, Δx (extension changes from both binding and unbinding events are combined for each data point; error bars denote s.e.m.). The grey shaded region shows a force-dependent long-polymer model $\Delta x_{\text{model}} = x_{ds}(F) - x_{ss}(F)$ using the XWLC model for $x_{ds}(F)$ and the SLC model for $x_{ss}(F)$ (see [37]). *Inset:* the four oligonucleotide probes used in this study (*bold*), bound to their complementary sequences on the tethered DNA (*not bold*). GC pairs are highlighted. Each oligonucleotide has a Cy3 fluorophore conjugated to its 3' end (*green disks*). (B) Extension changes due to hybridization of 9-nt probes to complementary sequences with varying numbers of spacers ($N_{sp} = 2, 1, 0$), scaled by probe length. *Inset:* the 9-nt probe (*bold*) bound to the three DNA constructs used in these experiments (*not bold*). GC pairs are highlighted. The probes used for binding the 2- and 1-spacer constructs have a Cy3 fluorophore (*green disks*) conjugated to their 3' ends, while the 9-nt probe used for binding the 0-spacer construct has a Cy3 fluorophore conjugated to an internal dT base to avoid steric clashes with the handles. (C) Extension changes due to hybridization of 10-nt probes of differing sequences, scaled by probe length. *Inset:* the three 10-nt probes used (*bold*), bound to their complementary sequences on the tethered DNA (*not bold*). GC pairs are highlighted. Each oligonucleotide has a Cy3 fluorophore conjugated to its 3' end (*green disks*).

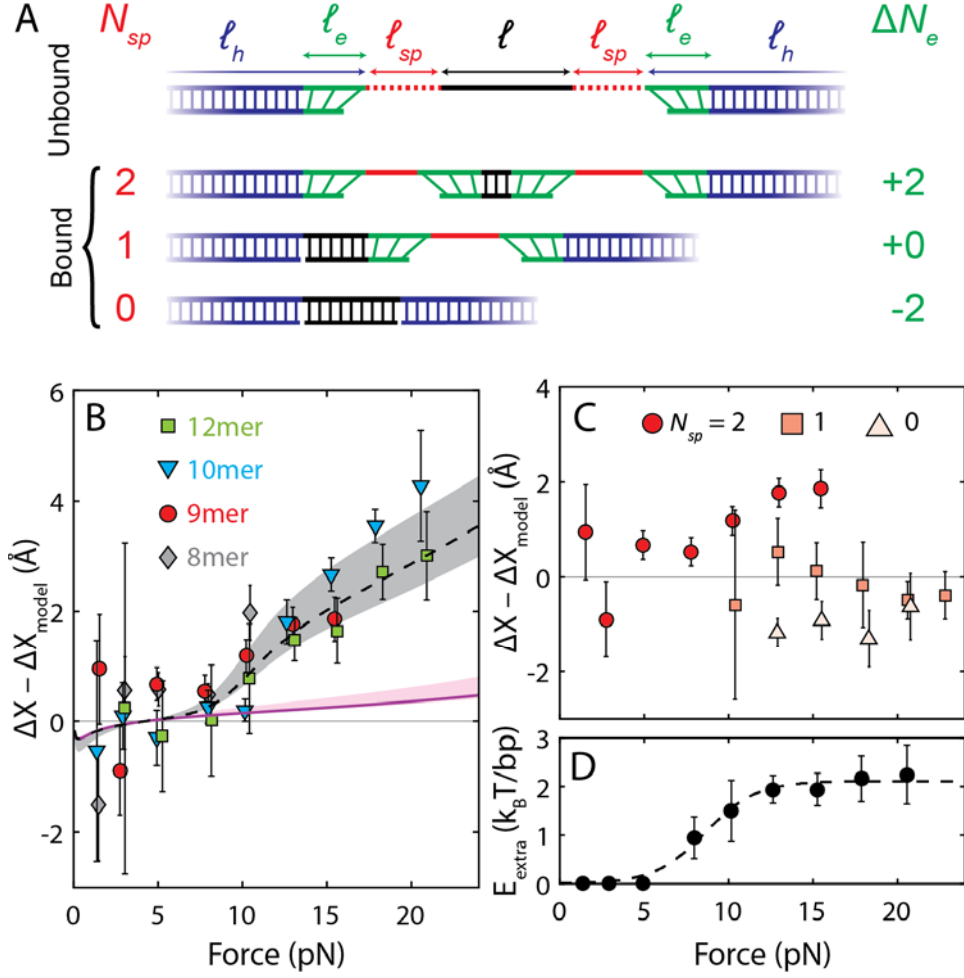


FIG. 3 (color online): Deviation of measured extension changes from long-polymer model. (A) Schematic of the DNA constructs used in this study and modeling of extension changes. *Top* (X_u): DNA construct with no probe bound. The dotted lines indicate a variable number of spacers ($N_{sp} = 2, 1, 0$) depending on the construct used. *Bottom three* (X_b): DNA constructs for varying number of spacers ($N_{sp} = 2, 1, 0$) with probe bound. *Blue*: dsDNA handles. *Green*: Duplex edge regions. *Red*: ssDNA poly-dT spacers. *Black*: Probe binding site and probe duplex region. (B) Residuals from extension change data for different probe lengths and long-polymer model, $\Delta X - \Delta X_{\text{model}}$, determined using optimal model parameters (see [37]). *Magenta line*: Fraying model of the duplex. Shaded area represents model over range of base-pairing energies for the different probes in (A); line represents model for average base-pairing energy. *Black dotted line*: Model for base-fraying with additional force-dependent energy term. Shaded area represents model over range of base-pairing energies for different probes in (A). (C) Residuals from extension change data of 9-nt probe binding to constructs with varying number of spacers ($N_{sp} = 2, 1, 0$). (D) Additional force-dependent energy required to destabilize edge base-pairs. *Black dotted line*: phenomenological model for force-dependence.

References

- [1] T. T. M. Ngo, Q. Zhang, R. Zhou, J. G. Yodh, and T. Ha, *Cell* **160**, 1135 (2015).
- [2] H. G. Garcia, P. Grayson, L. Han, M. Inamdar, J. Kondev, P. C. Nelson, R. Phillips, J. Widom, and P. A. Wiggins, *Biopolymers* **85**, 115 (2006).
- [3] K. Luger, A. W. Mader, R. K. Richmond, D. F. Sargent, and T. J. Richmond, *Nature* **389**, 251 (1997).
- [4] P. K. Purohit, J. Kondev, and R. Phillips, *Proceedings of the National Academy of Sciences of the United States of America* **100**, 3173 (2003).
- [5] Z. T. Berndsen, N. Keller, S. Grimes, P. J. Jardine, and D. E. Smith, *Proceedings of the National Academy of Sciences of the United States of America* **111**, 8345 (2014).
- [6] G. J. Wuite, S. B. Smith, M. Young, D. Keller, and C. Bustamante, *Nature* **404**, 103 (2000).
- [7] M. D. Wang, M. J. Schnitzer, H. Yin, R. Landick, J. Gelles, and S. M. Block, *Science* **282**, 902 (1998).
- [8] E. A. Galburt, S. W. Grill, A. Wiedmann, L. Lubkowska, J. Choy, E. Nogales, M. Kashlev, and C. Bustamante, *Nature* **446**, 820 (2007).
- [9] X. Qu, J.-d. Wen, L. Lancaster, H. F. Noller, C. Bustamante, and I. Tinoco, *Nature* **475**, 118 (2011).
- [10] T. Liu *et al.*, *eLife* **3**, e03406 (2014).
- [11] J.-D. Wen, L. Lancaster, C. Hodges, A.-C. Zeri, S. H. Yoshimura, H. F. Noller, C. Bustamante, and I. Tinoco, *Nature* **452**, 598 (2008).
- [12] G. Sirinakis, C. R. Clapier, Y. Gao, R. Viswanathan, B. R. Cairns, and Y. Zhang, *The EMBO Journal* **30**, 2364 (2011).
- [13] H. Dietz, S. M. Douglas, and W. M. Shih, *Science* **325**, 725 (2009).
- [14] C. E. Castro, H.-J. Su, A. E. Marras, L. Zhou, and J. Johnson, *Nanoscale* **7**, 5913 (2015).
- [15] T. E. Ouldridge, R. L. Hoare, A. A. Louis, J. P. K. Doye, J. Bath, and A. J. Turberfield, *ACS Nano* **7**, 2479 (2013).
- [16] J. J. Funke and H. Dietz, *Nature Nanotechnology* **11**, 47 (2015).
- [17] J. V. Le, Y. Luo, M. A. Darcy, C. R. Lucas, M. F. Goodwin, M. G. Poirier, and C. E. Castro, *ACS Nano* **10**, 7073 (2016).
- [18] P. C. Nickels, B. Wünsch, P. Holzmeister, W. Bae, L. M. Kneer, D. Grohmann, P. Tinnefeld, and T. Liedl, *Science* **354**, 305 (2016).
- [19] X. Wang and T. Ha, *Science* **340**, 991 (2013).
- [20] X. Wang, Z. Rahil, I. T. S. Li, F. Chowdhury, D. E. Leckband, Y. R. Chemla, and T. Ha, *Scientific Reports* **6**, 21584 (2016).
- [21] S. B. Smith, L. Finzi, and C. Bustamante, *Science* **258**, 1122 (1992).
- [22] C. Bustamante, J. Marko, E. Siggia, and S. B. Smith, *Science* **265**, 1599 (1994).
- [23] M. D. Wang, H. Yin, R. Landick, J. Gelles, and S. M. Block, *Biophysical Journal* **72**, 1335 (1997).
- [24] J. Camunas-Soler, M. Ribezzi-Crivellari, and F. Ritort, *Annual Review of Biophysics* **45**, 65 (2016).
- [25] T. E. Cloutier and J. Widom, *Proceedings of the National Academy of Sciences of the United States of America* **102**, 3645 (2005).
- [26] P. Wiggins, T. van der Heijden, F. Moreno-Herrero, A. Spakowitz, R. Phillips, J. Widom, C. Dekker, and P. Nelson, *Nature Nanotechnology* **1**, 137 (2006).
- [27] R. Vafabakhsh and T. Ha, *Science* **337**, 1097 (2012).
- [28] P. A. Wiggins, R. Phillips, and P. C. Nelson, *Physical Review E* **71**, 021909 (2005).
- [29] T. T. Le and H. D. Kim, *Nucleic Acids Research* **42**, 10786 (2014).
- [30] Q. Du, C. Smith, N. Shiffeldrim, M. Vologodskaya, and A. Vologodskii, *Proceedings of the National Academy of Sciences of the United States of America* **102**, 5398 (2005).
- [31] A. Vologodskii and M. D. Frank-Kamenetskii, *Nucleic Acids Research* **41**, 6785 (2013).

- [32] A. K. Mazur and M. Maaloum, *Nucleic Acids Research* **42**, 14006 (2014).
- [33] A. Mazur, *Physical Review Letters* **98**, 218102 (2007).
- [34] D. Ho, J. L. Zimmermann, F. a. Dehmelt, U. Steinbach, M. Erdmann, P. Severin, K. Falter, and H. E. Gaub, *Biophysical Journal* **97**, 3158 (2009).
- [35] K. Hatch, C. Danilowicz, V. Coljee, and M. Prentiss, *Physical Review E* **78**, 011920 (2008).
- [36] M. J. Comstock, T. Ha, and Y. R. Chemla, *Nature Methods* **8**, 335/340 (2011).
- [37] See Supplemental Material at [URL] for details on materials, experimental methods, and models, which includes Refs. [38]-[54].
- [38] T. Ha, *Methods* **25**, 78 (2001).
- [39] M. P. Landry, P. M. McCall, Z. Qi, and Y. R. Chemla, *Biophysical Journal* **97**, 2128 (2009).
- [40] I. Rasnik, S. A. McKinney, and T. Ha, *Nature Methods* **3**, 891 (2006).
- [41] Z. Qi, R. a. Pugh, M. Spies, and Y. R. Chemla, *eLife* **2**, e00334 (2013).
- [42] M. J. Comstock, K. D. Whitley, H. Jia, J. Sokoloski, T. M. Lohman, T. Ha, and Y. R. Chemla, *Science* **348**, 352 (2015).
- [43] M. C. Murphy, I. Rasnik, W. Cheng, T. M. Lohman, and T. Ha, *Biophysical Journal* **86**, 2530 (2004).
- [44] S. Suksombat, R. Khafizov, A. G. Kozlov, T. M. Lohman, and Y. R. Chemla, *eLife* **4**, e08193 (2015).
- [45] K. D. Whitley, M. J. Comstock, and Y. R. Chemla, *Nucleic Acids Research* **45**, 547 (2017).
- [46] S. V. Kuznetsov, Y. Shen, a. S. Benight, and A. Ansari, *Biophysical Journal* **81**, 2864 (2001).
- [47] C. Rivetti, C. Walker, and C. Bustamante, *Journal of Molecular Biology* **280**, 41 (1998).
- [48] S. B. Smith, Y. Cui, and C. Bustamante, *Science* **271**, 795 (1996).
- [49] J.-D. Wen, M. Manosas, P. T. X. Li, S. B. Smith, C. Bustamante, F. Ritort, and I. Tinoco, *Biophysical Journal* **92**, 2996 (2007).
- [50] N. C. Horton and B. C. Finzel, *Journal of Molecular Biology* **264**, 521 (1996).
- [51] K. D. Whitley, University of Illinois Urbana-Champaign, 2017.
- [52] S. Prakash and Y. Singh, *Physical Review E* **84**, 031905 (2011).
- [53] M. Mosayebi, A. A. Louis, J. P. K. Doye, and T. E. Ouldridge, *ACS Nano* **9**, 11993 (2015).
- [54] R. Owczarzy, B. G. Moreira, Y. You, M. A. Behlke, and J. A. Walder, *Biochemistry* **47**, 5336 (2008).
- [55] C. Bustamante, J. F. Marko, E. D. Siggia, and S. B. Smith, *Science* **265**, 1599 (1994).
- [56] O. A. Saleh, D. B. McIntosh, P. Pincus, and N. Ribeck, *Physical Review Letters* **102**, 068301 (2009).
- [57] P. Gross, N. Laurens, L. B. Oddershede, U. Bockelmann, E. J. G. Peterman, and G. J. L. Wuite, *Nature Physics* **7**, 731 (2011).
- [58] J. SantaLucia, *Proceedings of the National Academy of Sciences of the United States of America* **95**, 1460 (1998).
- [59] J. M. Huguet, C. V. Bizarro, N. Forns, S. B. Smith, C. Bustamante, and F. Ritort, *Proceedings of the National Academy of Sciences of the United States of America* **107**, 15431 (2010).
- [60] P. G. de Gennes, *Comptes Rendus de l'Academie des Sciences-Series IV* **2147**, 1505 (2001).
- [61] M. T. Woodside, W. M. Behnke-Parks, K. Larizadeh, K. Travers, D. Herschlag, and S. M. Block, *Proceedings of the National Academy of Sciences of the United States of America* **103**, 6190 (2006).
- [62] M. Rief, H. Clausen-schaumann, and H. E. Gaub, *Nature Structural Biology* **6**, 346 (1999).